

Reflection hologram recording in periodically poled LiNbO₃:Y:Fe

S Odoulov¹, A Shumelyuk¹, R Thien² and G von Bally²

¹ Institute of Physics, National Academy of Sciences, 03650, Kiev-39, Ukraine

² Laboratory of Biophysics, University of Münster, Robert-Koch-strasse 45, D-48149, Germany

E-mail: odoulov@iop.kiev.ua

Received 15 September 2003, accepted for publication 8 October 2003

Published 12 December 2003

Online at stacks.iop.org/JOptA/6/224 (DOI: 10.1088/1464-4258/6/2/012)

Abstract

Two counterpropagating light waves are used for recording reflection gratings in optical-damage-free lithium niobate crystals with a periodically alternating direction of the spontaneous polarization axis. In samples with the domain lattice vector aligned along the OX axis the reflection grating can be written only if the recording waves are tilted with respect to this axis. For a 1 mm thick sample a few per cent diffraction efficiency is achieved with ordinarily polarized recording and readout beams.

Keywords: dynamic holography, photorefraction, image recording

1. Introduction

Since the first publication on holographic grating recording in lithium niobate [1] that appeared in 1968, for years only perfectly poled single-domain crystals have been used for this purpose. Three years ago it was shown experimentally that multidomain ferroelectric photorefractive crystals may ensure the recording of high efficient holographic gratings, too [2], if the space charge formation is governed by the bulk photovoltaic effect [3, 4]. Moreover, multidomain crystals with a symmetric domain lattice, i.e. domains with one direction of spontaneous polarization are the same size as domains with the opposite orientation of spontaneous polarization, show an important advantage compared to bulk homogeneously poled material: they are free of optical damage [5] for laser beams with transverse dimensions much larger than the domain lattice period. This may allow us to overcome the serious drawbacks in the use of photorefractive crystals, e.g. for coherent metrological purposes and for archival optical data storage.

Until now only the recording of transmission gratings has been reported [1]. The parametric scattering that has been observed in periodically poled lithium niobate [6] was also a consequence of transmission grating recording [6, 7]. The purpose of this paper is to investigate whether PPLN samples are suitable for reflection grating recording and to find an optimized recording geometry for reflection grating recording.

2. Experiment

2.1. Experimental technique and PPLN samples

In the experiment the unexpanded light beams from the frequency doubled diode pumped Nd³⁺:YAG laser (single-mode, single-frequency, $\lambda = 0.53 \mu\text{m}$, 100 mW output power, approximately 1.5 mm beam waist in the sample) are used for holographic grating recording. A 1 mm thick sample is cut from a periodically poled lithium niobate (PPLN) crystal K243 synthesized in the Physics Department of Moscow State University. It contains 0.74 wt% of yttrium and 0.06 wt% of iron. Figure 1 represents the visualization of the domain structure: the relief of the chemically etched [010] face is shown by the grey density pattern. The input/output optically finished sample faces [100] are parallel to the domain walls; the axis of spontaneous polarization is parallel to the domain walls while the x axis is normal to the domain walls. The domain lattice period is approximately $L \approx 15 \mu\text{m}$.

Note that the iron content in the crystal K243 is ten times larger than in the crystal K-241 for which the suppression of optical damage was reported [2]. That is why at first the divergence of the single beam transmitted through the PPLN sample was checked: no increase in the beam spot in the far field was detected, neither with ordinarily polarized nor with extraordinarily polarized light.

In grating recording experiments two recording beams (with wavevectors \mathbf{k}_1 and \mathbf{k}_2) impinge upon the sample in the XOZ plane, OZ being the axis of spontaneous polarization

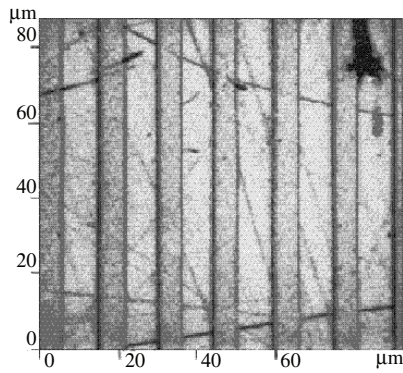


Figure 1. Image of the etched [010] face of PPLN:Fe:Y showing the periodic domain structure.

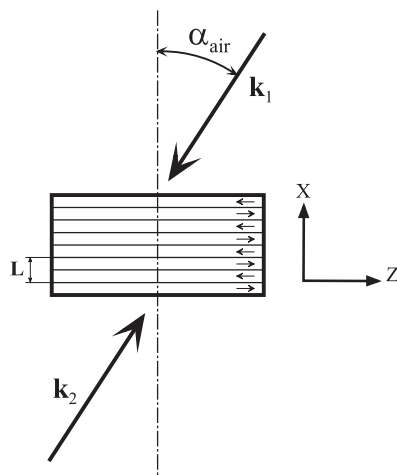


Figure 2. Schematic representation of reflection grating recording with two counterpropagating light waves. \mathbf{k}_1 and \mathbf{k}_2 are the wavevectors. Arrows inside each domain indicate the direction of spontaneous polarization.

and OX normal to the domain walls (see figure 2). The two waves are polarized identically, either normal to the XOZ plane (ordinary waves) or in the XOZ plane (extraordinary waves). They can be tilted to a certain angle α_{air} roughly within the interval $-60^\circ \leq \alpha_{\text{air}} \leq 60^\circ$. For any particular tilt angle a grating is recorded until saturation (which usually takes several minutes) and then its diffraction efficiency is measured with only one of the two recording waves as a ratio of the diffracted signal intensity to the total intensity of the transmitted and diffracted beams. The experimental procedure is similar to that used to study reflection hologram recording in bulk homogeneously poled iron-doped lithium niobate [8].

2.2. Experimental results

In the standard geometry for reflection grating recording in LiNbO₃ the grating vector $\mathbf{K} = \mathbf{k}_1 - \mathbf{k}_2$ is aligned along the OZ direction [8]. For PPLN used in the present experiments this is an unfavourable orientation because of the considerable diffraction of the recording light from the charged domain walls. For the same reason the recording of a grating with \mathbf{K} along the OY axis is undesirable. Therefore, we started with recording by waves aligned along the OX axis (i.e. normal to the domain walls) or tilted in the XOZ plane.

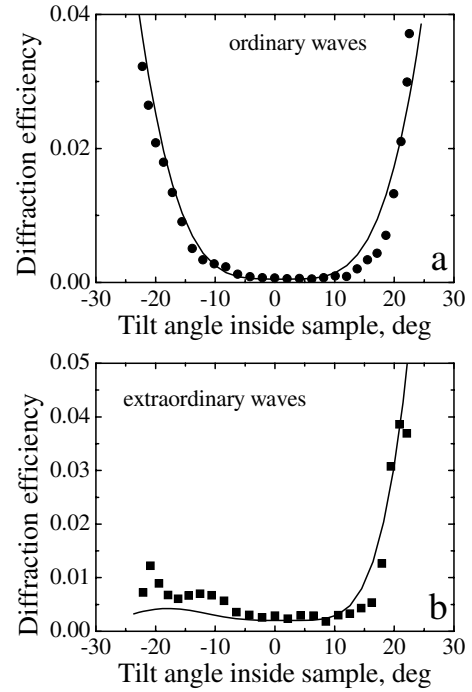


Figure 3. Angular dependence of the diffraction efficiency for recording and readout with ordinarily polarized waves (a) and with extraordinarily polarized waves (b). Full curves represent the fit of the calculated dependences (see discussion).

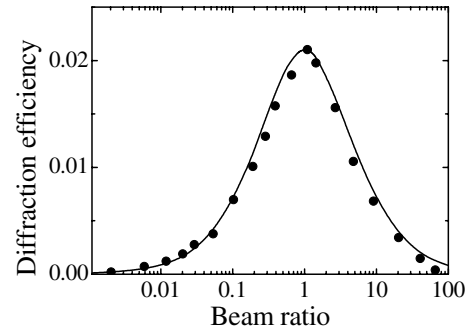


Figure 4. Beam ratio dependence of the diffraction efficiency for recording and reconstruction with ordinarily polarized waves and $\alpha_{\text{air}} = 60^\circ$. The full curve represents the fit of the calculated dependences (see discussion).

Figures 3(a) and (b) show the measured angular dependence of the diffraction efficiency for two polarizations of the recording and readout waves, ordinary and extraordinary, respectively. Here α stands for the angle between the sample face normal and the light propagation direction inside the sample and is related to α_{air} according to the refraction law. In both cases the diffraction efficiency at normal incidence $\alpha = 0$ is close to its minimum value. The dependence for extraordinary waves is obviously asymmetric while the dependence for ordinary waves is roughly symmetric. The largest diffraction efficiency achieved is 0.04.

Adjusting a fixed $\alpha_{\text{air}} = 60^\circ$ we measure the dependence of the diffraction efficiency on the beam intensity ratio. A typical bell-shaped dependence is obtained with the maximum at the highest possible fringe contrast (figure 4).

The image bearing beams were also used for hologram recording. Figure 5(a) shows the reconstructed image

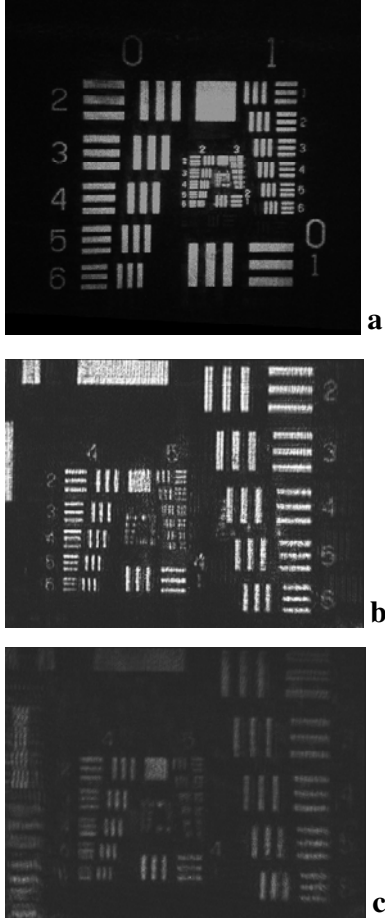


Figure 5. Image of an USAF resolution chart reconstructed from a reflection hologram recorded with ordinarily polarized light waves in PPLN:Fe:Y (a). Magnified fragment of the image transmitted through the PPLN:Fe:Y sample (b) and reconstructed image of this fragment (c).

of a complete USAF resolution chart. The fragment of the magnified image transmitted through the PPLN sample is shown in figure 5(b) and the image of this fragment reconstructed from the reflection hologram is presented in figure 5(c). The bars of element 6 of group 4 ($28.5 \mu\text{m}$) are well resolved. The comparison of figures 5(b) and (c) shows that the resolution is limited not by the PPLN crystal itself but by the quality of the optics used for image formation.

3. Discussion

Two coherent light waves with the electric fields

$$\begin{aligned} \mathbf{E}_1 &= \mathbf{e}_1 A_1 \exp(i\mathbf{k}_1 \mathbf{r}) \\ \mathbf{E}_2 &= \mathbf{e}_2 A_2 \exp(i\mathbf{k}_2 \mathbf{r}) \end{aligned} \quad (1)$$

that impinge upon the sample produce intensity fringes if the polarization unit vectors \mathbf{e}_ℓ meet the condition $\mathbf{e}_1 \cdot \mathbf{e}_2 = 1$ and/or of the polarization fringes if this condition is violated. Here A_ℓ stands for the complex amplitudes of the light waves, \mathbf{k}_ℓ for the wavevector of each wave and \mathbf{r} for the propagation vector. This spatial modulation of the light intensity or polarization results in the excitation of a spatially modulated

photovoltaic current:

$$j_i = \beta_{ijk} \mathbf{E}_j \mathbf{E}_k^*, \quad (2)$$

where β_{ijk} is a third rank photovoltaic tensor [4] and $\mathbf{E} = \mathbf{E}_1 + \mathbf{E}_2$ is the electric field of two waves. In turn, the photovoltaic current redistributes charges inside the sample and leads to the appearance of a space-charge grating with the grating vector $\mathbf{K} = \mathbf{k}_1 - \mathbf{k}_2$. The static electric field of this space-charge grating is

$$\mathbf{E}^{\text{sc}}(r) = \mathbf{j}(r)/\sigma, \quad (3)$$

and it modulates the high frequency dielectric tensor:

$$\Delta \hat{\epsilon}_{\ell m}^{-1} \propto r_{\ell mn} E_n^{\text{sc}} \quad (4)$$

i.e. the volume phase grating appears. Here $r_{\ell mn}$ is a third rank tensor of the linear electrooptic effect (Pockels effect) and σ is the crystal photoconductivity.

For small phase modulation, $(\pi \Delta n \ell / \lambda) \ll 1$, the diffraction efficiency of a grating is proportional to the light-induced change of the high frequency electric permittivity (see, for example, [9]):

$$\eta \propto (\Delta n)^2 \propto (\Delta \epsilon)^2. \quad (5)$$

Here ℓ is the sample thickness. In turn, $\Delta \epsilon$ is proportional to the product of the effective electrooptic and photovoltaic coefficients (see equations (4), (3) and (2)):

$$\Delta \epsilon \propto (r_{\text{eff}} \beta_{\text{eff}}). \quad (6)$$

The last equation allows us to explain qualitatively why an efficient grating recording is possible even in multidomain ferroelectrics with the bulk photovoltaic effect. The signs of both tensor components, r_{eff} and β_{eff} , are sensitive to the inversion of the spontaneous polarization direction; the sign of the product $(r_{\text{eff}} \beta_{\text{eff}})$ remains, however, the same in every two adjacent domains with opposite orientations of the axis of spontaneous polarization. This leads to an important consequence for photorefractive gratings: there is no spatial shift between the gratings recorded in adjacent domains. The structure of the index grating recorded in a multidomain crystal repeats, to a first approximation, the intensity distribution in the fringe pattern. The only difference compared to the bulk homogeneously poled sample consists in a complete cancellation of the space charge field (and therefore of refractive index variation) in close vicinity to the domain walls. Intuitively it is clear that, with increasing period of the domain lattice, the effect of the domain walls will become smaller.

The theory predicts that the space charge field in periodically poled lithium niobate with photovoltaic charge transport reaches its largest possible value (the same as in a homogeneously poled crystal) if the grating spacing Λ becomes much smaller than the domain lattice period L [10, 11]. The calculated first Fourier harmonic of the space charge field (responsible for index grating which is Bragg-matched to the recording waves) in periodically poled crystals with photovoltaic charge transport is

$$\mathbf{E}_{\mathbf{K}} = -\mathbf{n}_z E_{\text{pv}} [1 - (2G/\pi K) \tanh(\pi K/2G)], \quad (7)$$

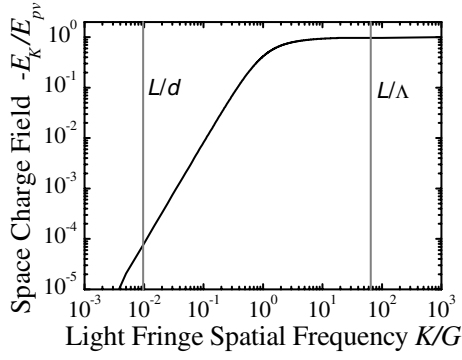


Figure 6. Calculated dependence of space charge field on normalized grating spatial frequency. The vertical lines show the spatial frequency of the grating (with the grating spacing $0.1 \mu\text{m}$) and that for an expanded laser beam (with the beam waist 1.5 mm).

where $G = 2\pi/L$ is the spatial frequency of the domain lattice, $K = 2\pi/\Lambda$ is the spatial frequency of the recording fringes and E_{pv} is an effective photovoltaic field [4]. The calculation was performed for a transmission grating geometry with the grating vector parallel to the OZ axis (unit vector \mathbf{n}_z) under the assumption that E_{pv} is much smaller than the trap density limited space charge field.

The normalized space charge field E_K/E_{pv} is plotted in figure 6 as a function of the normalized spatial frequency (K/G). For small fringe spacing (large K/G) the space charge field E_K approaches its ultimate value E_{pv} that can be reached in a single-domain crystal while for large scale intensity variation ($K \ll G$) E_K is decreasing as [9, 10] $E_K \propto (K/G)^2$. We believe this conclusion is valid for arbitrary mutual orientation of the photorefractive grating vector \mathbf{K} and domain grating vector \mathbf{G} including $\mathbf{K} \parallel \mathbf{G}$. We also suppose that space charge limitations will not strongly reduce the space charge field in our PPLN sample with a relatively large density of iron impurity.

Let us consider now the angular dependences of the crystal response to compare them with the experimentally measured data. The general expressions for efficient electrooptic constant and efficient photovoltaic constant are as follows:

$$r_{\text{eff}} = r_{kmn} e_k^\gamma e_m^\delta \nu_n \quad (8)$$

and

$$\beta_{\text{eff}} = \beta_{ij\ell} \nu_i e_j^\alpha e_\ell^\beta \quad (9)$$

where e_p^ζ are the components of the polarization unit vectors of the recording waves, superscripts $\zeta = 1$ and 2 denote waves 1 and 2, respectively, and subscripts $p = 1, 2,$ and 3 correspond to the Cartesian components of the grating unit vector, $\nu = \mathbf{K}/|\mathbf{K}|$.

For LiNbO₃ the real part of the photovoltaic tensor (symmetric in the last two indices) has four independent components [4]: $\beta_{333}, \beta_{311} = \beta_{322}, \beta_{222} = \beta_{211} = \beta_{121}$ and $\beta_{131}^s = \beta_{113}^s$. The structure of the electrooptic tensor is similar to that of the photovoltaic tensor and the principal nonvanishing components are $r_{333}, r_{113} = r_{223}, r_{222} = r_{112} = r_{121}$ and $r_{131} = r_{311}$ [12]. Among all the mentioned tensor components the smallest are β_{131}^s and β_{222} for the photovoltaic effect and r_{222} for the electrooptic effect of LiNbO₃:Fe. These components

will be neglected in our further considerations. Contracted indices will be used for tensor components, with the two indices referring to light polarization replaced by only one according to the following rules: $33 \rightarrow 3, 22 \rightarrow 2, 11 \rightarrow 1, 21 \rightarrow 6, 31 \rightarrow 5$ and $32 \rightarrow 4$.

For the recording and readout with ordinarily polarized light waves the expressions for the effective electrooptic and photovoltaic coefficients are rather simple:

$$r_{\text{eff}} = r_{13} \sin \alpha \quad (10)$$

$$\beta_{\text{eff}} = \beta_{31} \sin \alpha. \quad (11)$$

As the diffraction efficiency is proportional, according to equations (7) and (8), to

$$\eta \propto (\Delta n)^2 \propto (r_{\text{eff}} \beta_{\text{eff}})^2, \quad (12)$$

we obtain the angular dependence

$$\eta \propto (r_{13} \beta_{31})^2 \sin^4 \alpha. \quad (13)$$

The full curve in figure 3(a) represents a fit of equation (13) to the experimental dependence. Apart from the proportionality constant in equation (13) two other fitting parameters are introduced: a possible misalignment of the sample faces with respect to the OZ axis (the fit gives the value $\Delta \alpha \approx 2^\circ$) and background scattering that increases η values, especially in the vicinity of $\alpha = 0$, where the efficiency is negligibly small ($\Delta \eta \approx 0.0005$).

For the recording and readout with extraordinarily polarized light waves the expressions for the effective electrooptic and photovoltaic coefficients are more complicated:

$$r_{\text{eff}} = (r_{33} \cos^2 \alpha + r_{13} \sin^2 \alpha - 2r_{51} \sin \alpha \cos \alpha) \sin \alpha \quad (14)$$

$$\beta_{\text{eff}} = (\beta_{33} \cos^2 \alpha + \beta_{31} \sin^2 \alpha - 2\beta_{15}^s \sin \alpha \cos \alpha) \sin \alpha. \quad (15)$$

For the angular dependence of the diffraction efficiency we therefore obtain

$$\eta \propto (r_{13} \beta_{31})^2 \sin^4 \alpha \left[\cos^4 \alpha + \frac{r_{13} \beta_{31}}{r_{33} \beta_{33}} \sin^4 \alpha + \left(\frac{r_{13}}{r_{33}} + \frac{\beta_{31}}{\beta_{33}} + 4 \frac{r_{51} \beta_{15}^s}{r_{33} \beta_{33}} \right) \sin^2 \alpha \cos^2 \alpha - 2 \left(\frac{r_{51}}{r_{33}} + \frac{\beta_{15}^s}{\beta_{33}} \right) \sin \alpha \cos^3 \alpha - 2 \left(\frac{r_{51} \beta_{31}}{r_{33} \beta_{33}} + \frac{\beta_{15}^s r_{13}}{\beta_{33} r_{33}} \right) \sin^3 \alpha \cos \alpha \right]^2. \quad (16)$$

To fit these relations to the experimental data of figure 3(b) one needs to know at least the ratios of the electrooptic tensor components to those of the photovoltaic tensor components. Under the assumption that the presence of a large amount of Y in our sample does not affect the ratios of the photovoltaic coefficients we use the following data [8, 12–14]:

$$\begin{aligned} \frac{r_{13}}{r_{33}} &\simeq 0.24 \\ \frac{\beta_{31}}{\beta_{33}} &\simeq 1.2 \\ \frac{r_{51}}{r_{33}} &\simeq 0.9. \end{aligned} \quad (17)$$

The terms with β_{15}^s/β_{33} show negligible values.

When fitting equation (16) to the experimental data we referred to the already known error in alignment of the sample faces $\Delta\alpha \approx 2^\circ$. The full curve in figure 3(b) represents the result of the fit. As the beam fanning is always larger for extraordinary waves than for the ordinary ones the fit gives a larger amount for the background signal, $\Delta\eta \approx 0.002$. It is obvious that it describes reasonably well the measured dependence.

The beam ratio dependence (figure 4) may be well fitted by a standard dependence typical for all media with a local nonlinear response [15]:

$$\eta = \eta_{\max} \frac{4m}{(1+m)^2} \quad (18)$$

where m is the recording beam intensity ratio. This confirms the initial assumption about the local nonlinear response of PPLN which is due to photovoltaic charge transport.

4. Conclusion

It is proved experimentally that periodically poled iron doped lithium niobate crystals can be used successfully for the recording of reflection gratings.

The anisotropy of the photorefractive response that is due to the tensor properties of the electrooptic effect and the photovoltaic effect does not allow for recording and reconstruction of a reflection grating with the grating vector parallel to the crystal OX axis. The tilt of the sample to rather large angles, up to 60° in air with respect to this axis, allows us to reach a diffraction efficiency of 0.04.

The measured angular dependences for diffraction efficiency that are in reasonably good agreement with the calculated ones show a tendency for increasing efficiency when the grating vector has a larger z -axis component. To optimize the reflection grating recording it would be desirable to synthesize PPLN structures with a lattice vector along the axis of spontaneous polarization. The other, less efficient, option is to use PPLN with spontaneous polarization tilted with respect to the domain walls or to cut available crystals at a certain angle to the domain walls.

These results show the possibilities for high resolution imaging as well as for information storage in photorefractive crystals.

Acknowledgments

This work has been supported by the Alexander von Humboldt Foundation in the framework of the Research Award to SO and by the German Ministry of Education and Research (project no 13N8183). We are grateful to Dr Inna Naumova (Moscow State University) for PPLN samples, to Dr Pierre Mathey (Université de Bourgogne) for domain structure visualization and to Professor B Sturman (Institute of Automatization and Electrometry, Novosibirsk) for fruitful discussions.

References

- [1] Chen F S, La Macchia J T and Fraser D B 1968 *Appl. Phys. Lett.* **13** 223
- [2] Odoulov S, Tarabrova T, Shumelyuk A, Naumova I I and Chaplina T O 2000 *Phys. Rev. Lett.* **84** 3294
- [3] Glass A M, von der Linde D and Negran T K 1974 *Appl. Phys. Lett.* **25** 233
- [4] Sturman B I and Fridkin V M 1992 *The Photovoltaic and Photorefractive Effects in Noncentrosymmetric Materials* (Philadelphia, PA: Gordon and Breach)
- [5] Ashkin A, Boyd C D, Dziedzic J M, Smith R G, Ballman A A, Levinstein J J and Nassau K 1966 *Appl. Phys. Lett.* **9** 72
- [6] Gouklov M, Odoulov S, Naumova I, Agulló-López F, Calvo G, Podivilov E, Sturman B and Pruneri V 2001 *Phys. Rev. Lett.* **86** 4021
- [7] Podivilov E V, Sturman B I, Gouklov M, Odoulov S, Calvo G, Agulló-López F and Carrascosa M 2002 *J. Opt. Soc. Am. B* **19** 1582
- [8] Riehemann S, von Bally G, Sturman B and Odoulov S 1997 *Appl. Phys. B* **65** 535
- [9] Taya M, Bashew M C and Fejer M M 1996 *Opt. Lett.* **21** 857
- [10] Sturman B, Aguilar M, Agulló-López F, Pruneri V and Kazansky P G 1997 *J. Opt. Soc. Am. B* **14** 2641
- [11] Petrov M P, Stepanov S I and Khomenko A V 1991 *Photorefractive Crystals in Coherent Optical Systems* (Berlin: Springer)
- [12] Wemple S H, Domenico M Di and Camlibel J 1968 *J. Chem. Solid* **29** 1797
- [13] Festl H G, Hertel P, Kraetzig E and von Balz R 1982 *Phys. Status Solidi b* **113** 157
- [14] Odoulov S 1989 *Ferroelectrics* **91** 213
- [15] Kukhtarev N, Markov V, Odoulov S, Soskin M and Vinetski V 1972 *Ferroelectrics* **22** 961